

# Discontinuous Galerkin solution of preconditioned Euler equations for very low Mach number flows

A. Nigro<sup>1</sup>, C. De Bartolo<sup>1,\*</sup>, R. Hartmann<sup>2</sup>, F. Bassi<sup>3</sup>

<sup>1</sup> *Dip. di Meccanica-Università della Calabria Ponte P. Bucci cubo 44/C 87036 - Rende (CS), Italy.*

<sup>2</sup> *Institute of Aerodynamics and Flow Technology, German Aerospace Center (DLR), Lilienthalplatz 7, 38108 Braunschweig, Germany.*

<sup>3</sup> *Dip. di Ingegneria Industriale-Università di Bergamo viale Marconi 5 24044 - Dalmine (BG), Italy.*

## SUMMARY

In this work we present a Discontinuous Galerkin (DG) method designed to improve the accuracy and efficiency of the steady-state solution at very low Mach number flows using an explicit scheme. The algorithm is based on a perturbed formulation of the compressible Euler equations and employs the preconditioning of both the instationary term of the governing equations and the dissipative term of the numerical flux function (full preconditioning approach).

The performance of the scheme is demonstrated by solving an inviscid flow past a NACA0012 airfoil at different very low Mach numbers using various degrees of polynomial approximation. We present numerical results computed with and without perturbed variables which illustrate the influence of the cancellation errors on both the convergence and the accuracy of the DG solutions at low Mach numbers. Copyright © 2000 John Wiley & Sons, Ltd.

---

\*Correspondence to: c.debartolo@unical.it, Dip. di Meccanica-Università della Calabria Ponte P. Bucci cubo 44/C 87036 - Rende (CS), Italy.

19 KEY WORDS: Discontinuous Galerkin finite element method; Low Mach number; Cancellation error;  
20 Preconditioning; Euler equations.

21

22

## 1. INTRODUCTION

23 DG methods have received more and more attention in the last years because of their appealing  
24 features that justify the widespread applications of these methods. In particular, the minimal amount  
25 of numerical dissipation and the potential to reduce the gridding requirements and the time necessary  
26 to achieve a desired accuracy level of DG solutions, make this method very appealing for low Mach  
27 number flow computations [1, 2].

28 The difficulty in solving the compressible Euler equations at low Mach number is due to the large  
29 disparity of wave speeds. Well known, undesirable effects of low speed flow on most numerical  
30 schemes include low convergence speed and loss of accuracy, [3, 4, 5]. Another issue related to the  
31 numerical solution of low speed flows concerns the careful implementation of non-reflecting boundary  
32 conditions [6, 7, 8].

33 Several preconditioning techniques, applied to the governing equations and to their discretizations,  
34 have been developed in the past to cope with the stiffness and accuracy problems [6, 9, 10, 11]. These  
35 techniques basically scale the wave speeds to the same order of magnitude premultiplying the time  
36 derivative terms of the governing equations by a preconditioning matrix. For the large family of upwind  
37 schemes, preconditioning enters also in the formulation of numerical flux functions in order to properly  
38 balance the artificial dissipation implied by the numerical flux formulation, [4, 5, 12]. Some of the most  
39 recognized local preconditioners for inviscid and viscous flows were proposed by Turkel [9, 10], Lee  
40 and van Leer [11], Weiss and Smith [13] and Choi and Merkle [14].

41 Recently, Nigro in [15] and [16] introduced the low Mach number preconditioning for DG  
 42 discretizations and reported for Mach numbers down to  $M = 10^{-3}$  that the preconditioning technique  
 43 results in a significant improvement of the convergence speed. Furthermore, it has been shown that  
 44 preconditioning enhances the accuracy of numerical solutions.

45 Nevertheless, it is difficult or impossible to solve Euler equations at very low Mach numbers even  
 46 with preconditioning. This is due to cancellation errors which occur as an accumulation effect of  
 47 round-off errors. Round-off errors depend mainly on the floating point representation used and are  
 48 thus unavoidable.

49 The problem of the cancellation error can be minimized by formulating the governing equations  
 50 in terms of perturbed variables [17, 18]. Reference quantities are introduced in the equations for the  
 51 thermodynamic variables and the computations are performed for the fluctuations.

52 The governing equations are unaltered and the method can be used in conjunction with standard  
 53 numerical strategies, like preconditioning. Several previous studies [14, 19, 20, 21, 22] showed that  
 54 this problem can be alleviated by employing the concept of gauge pressure, in which the pressure is  
 55 decomposed into a constant reference pressure and a relative pressure. Sesterhenn et al. [17] extended  
 56 the relative treatment to all variables and flux vectors. Nevertheless, Lee [23] showed that this approach  
 57 produced a slight improvement in the convergence process of the energy equation while the precision  
 58 of floating-point variables was a much more important factor in the calculations of the temperature  
 59 field at very low Mach numbers. Usually, double precision allows to circumvent the problem of  
 60 cancellation errors for engineering accuracy. Notwithstanding, this floating point representation cannot  
 61 be sufficient to obtain higher accurate results: the higher the accuracy of solution, the larger the number  
 62 of computations with round-off error occurring at each computation. Thus, the perturbed formulation of  
 63 the governing equations becomes mandatory to obtain a highly accurate representation of the unknowns

64 at low Mach numbers using higher order schemes.

65 Finally, concerning the set of dependent variables, it has been shown in [24] that the conservative  
66 incompressible formulation is well defined only for the entropy variables and the primitive variables  
67 including pressure. It has also been shown that these two sets of variables are best suited for solving  
68 practical problems, with the primitive variables being more accurate than the entropy variables for  
69 low speed and incompressible flow computations. For these reasons the primitive variables are often  
70 preferred for low Mach number computations [13, 14, 23, 25] and they have also been used to develop  
71 numerical schemes well suited for both compressible and incompressible flows.

72 In this paper we present a preconditioned DG discretization of the 2D compressible Euler equations  
73 suitable to compute inviscid very low Mach number flows. The preconditioning affects both the time  
74 derivative terms of the governing equations, through the action of the Weiss and Smith preconditioning  
75 matrix [13], and the numerical dissipation of the Roe's Riemann solver used to compute the numerical  
76 flux (full preconditioning technique). The method is applicable only to steady-state simulations as  
77 the preconditioning of the unsteady terms destroys the time accuracy of the governing equations. The  
78 conservative system of equations is written in terms of perturbed variables and iterated to steady state  
79 using an explicit scheme.

80 This paper aims at giving a contribution on developing a conservative DG scheme that is suitable  
81 for compressible and incompressible flows. In particular, here we extend the DG discretization of the  
82 Euler equations, written in the most appropriate set of primitive variables, to the incompressible limit,  
83 we consider the relationships between convergence characteristics and the Mach number for different  
84 degrees of polynomial approximation, and, finally, we examine the influence of the cancellation error  
85 on both the accuracy of solutions and the convergence characteristics, taking into account the effect of  
86 the polynomial degree.

87 The outline of the paper is as follows. In Section 2 we present the preconditioned form of  
 88 the compressible Euler equations using primitive variables and perturbed variables. In Section 3  
 89 we describe the DG discretization of the governing equations, the boundary conditions and the  
 90 preconditioned numerical flux function. In Section 4 we give some details on the explicit time stepping  
 91 scheme. The performance of the numerical scheme is then demonstrated in Section 5 by computing an  
 92 inviscid flow around a NACA0012 airfoil for different very low Mach numbers (down to  $M = 10^{-15}$ )  
 93 and different degrees of polynomial approximation ( $P = 1, 2, 3$ ). Finally, a few conclusions are drawn  
 94 in Section 6.

## 95 2. GOVERNING EQUATIONS

### 96 2.1. The preconditioned compressible Euler equations

97 We consider the preconditioned two-dimensional compressible Euler equations in conservative form,

$$\Gamma \frac{\partial \mathbf{q}}{\partial t} + \nabla \cdot \mathbf{F} = 0. \quad (1)$$

98 The primitive variables  $\mathbf{q}$  and the cartesian components  $\mathbf{f}$  and  $\mathbf{g}$  of the flux function  $\mathbf{F}$  are given by:

$$\mathbf{q} = \begin{pmatrix} p \\ u \\ v \\ T \end{pmatrix}, \quad \mathbf{f} = \begin{pmatrix} \rho u \\ \rho u^2 + p \\ \rho uv \\ \rho Hu \end{pmatrix}, \quad \mathbf{g} = \begin{pmatrix} \rho v \\ \rho vu \\ \rho v^2 + p \\ \rho Hv \end{pmatrix}, \quad (2)$$

99 where  $p$  is the pressure,  $T$  is the fluid temperature,  $u$  and  $v$  are the velocity components,  $\rho$  is the  
 100 density and  $H$  is the total enthalpy per unit mass. By assuming that the fluid obeys the perfect gas state  
 101 equation,  $H$  is given by  $H = c_p T + 0.5(u^2 + v^2)$ , where  $c_p$  denotes the isobaric specific heat capacity

102 of the fluid, and  $\rho$  can be calculated as  $\rho = p/T$ .

103 The matrix  $\Gamma$  used in the present work is the local preconditioning matrix of Weiss and Smith [13]  
 104 written in the following form

$$\Gamma = \begin{pmatrix} \Theta & \rho_T & 0 & 0 \\ \Theta u & \rho_T u & \rho & 0 \\ \Theta v & \rho_T v & 0 & \rho \\ \Theta H - 1 & \rho_T H + \rho c_p & \rho u & \rho v \end{pmatrix}, \quad (3)$$

105 where  $\rho_T = \left. \frac{\partial \rho}{\partial T} \right|_{p=\text{const.}}$  and  $\Theta$  is given by

$$\Theta = \left( \frac{1}{U_r^2} - \frac{\rho_T}{\rho c_p} \right). \quad (4)$$

106 Here,  $U_r$  is a reference velocity which, for an ideal gas, is defined as

$$U_r = \begin{cases} \varepsilon c, & \text{if } |\mathbf{v}| < \varepsilon c, \\ |\mathbf{v}|, & \text{if } \varepsilon c < |\mathbf{v}| < c, \\ c, & \text{if } |\mathbf{v}| > c, \end{cases} \quad (5)$$

107 where  $c$  is the acoustic speed and  $\varepsilon$  is a small number included to prevent singularities at stagnation  
 108 points. Furthermore, by assuming that the fluid obeys the perfect gas state equation,  $\rho_T$  can be  
 109 calculated as  $\rho_T = -\rho/T$ . Choosing  $\varepsilon = O(M)$ , the low Mach preconditioning ensures that the  
 110 convective and acoustic wave speeds are of similar magnitude, proportional to the flow speed [26].

111 In the next section we will show how preconditioning enters in the formulation of the numerical  
 112 flux function in the normal direction at Gauss integration points on inter-element faces. Hence it is  
 113 worthwhile introducing here the wave speeds of the preconditioned Euler equations in the direction of  
 114 the unit vector  $\mathbf{n}$ , which are given by the eigenvalues of  $\Gamma^{-1}(\frac{\partial \mathbf{f}}{\partial \mathbf{q}} n_1 + \frac{\partial \mathbf{g}}{\partial \mathbf{q}} n_2)$ , where  $\frac{\partial \mathbf{f}}{\partial \mathbf{q}}$  and  $\frac{\partial \mathbf{g}}{\partial \mathbf{q}}$  are the

115 inviscid flux jacobians with respect to the primitive variables, and  $n_1$  and  $n_2$  are the components of the  
 116 unit vector  $\mathbf{n} = (n_1, n_2)^T$ . The propagation speeds in this direction are

$$\lambda_1 = \lambda_2 = u_n, \quad \lambda_3 = u'_n + c', \quad \lambda_4 = u'_n - c',$$

117 where

$$\begin{aligned} u_n &= \mathbf{v} \cdot \mathbf{n}, \\ u'_n &= u_n(1 - \alpha), \\ c' &= \sqrt{\alpha^2 u_n^2 + U_r^2}, \\ \alpha &= \frac{1 - \beta U_r^2}{2}, \\ \beta &= \left( \rho_p + \frac{\rho_T}{\rho c_p} \right), \\ \rho_p &= \left. \frac{\partial \rho}{\partial p} \right|_{T=\text{const.}}. \end{aligned} \tag{6}$$

For an ideal gas  $\rho_p = 1/T$  and  $\beta = 1/c^2$ . At low speed as  $U_r \rightarrow 0$ ,  $\alpha \rightarrow 1/2$ , and all the eigenvalues become of the same order as  $u_n$ . We note that all the above equations have been written in non-dimensional form using the dimensional relationships with the reference values of length  $l_r$ , density  $\rho_r$ , pressure  $p_r$  and gas constant  $R_r$ . The non-dimensionalized quantities have the following orders of magnitude:

$$\begin{aligned} p, \rho, T &\sim O(1), \quad u, v, u_n \sim O(M), \quad H, c_p \sim O(1), \\ u'_n, c' &\sim O(M), \quad \Theta \sim O(M^{-2}). \end{aligned} \tag{7}$$

## 118 2.2. Perturbed variables

119 In this work the relative thermodynamic dependent variables  $p'$  and  $T'$  are defined as,

$$\begin{aligned} p' &= p - p_\infty \\ T' &= T - T_\infty \end{aligned} \quad (8)$$

where  $p_\infty$  and  $T_\infty$  are the freestream pressure and temperature respectively. Furthermore the momentum fluxes are defined considering the relative pressure,  $p'$ . Then the primitive variables  $\mathbf{q}$  and the cartesian components  $\mathbf{f}$  and  $\mathbf{g}$  of the convective flux function  $\mathbf{F}$  are given as follows,

$$\mathbf{q} = \begin{bmatrix} p' \\ u \\ v \\ T' \end{bmatrix}; \quad \mathbf{f} = \begin{bmatrix} \rho u \\ \rho u u + p' \\ \rho u v \\ \rho H u \end{bmatrix}; \quad \mathbf{g} = \begin{bmatrix} \rho v \\ \rho v u \\ \rho v v + p' \\ \rho H v \end{bmatrix}. \quad (9)$$

The perturbed formulation of the preconditioned governing equations obtained using Eq.(9) is mathematically equivalent to the original one, Eq.(1). In particular, the preconditioning matrix, Eq.(3), is not modified and the ideal gas law is maintained.

### 3. THE PRECONDITIONED DG DISCRETIZATION

Multiplying Eq. (1) by a vector-valued test function  $\mathbf{v}$  and integrating by parts, we obtain the weak formulation:

$$\int_{\Omega} \mathbf{v}^T \Gamma \frac{\partial \mathbf{q}}{\partial t} d\mathbf{x} - \int_{\Omega} \nabla \mathbf{v}^T \cdot \mathbf{F} d\mathbf{x} + \int_{\partial\Omega} \mathbf{v}^T \mathbf{F} \cdot \mathbf{n} ds = 0 \quad \forall \mathbf{v} \in H^1(\Omega) \quad (10)$$

where  $\Omega$  is the domain with boundary  $\partial\Omega$ , and  $\mathbf{n}$  is the unit outward normal vector. To discretize in space, we define  $\mathbf{V}_h^p$  to be the space of discontinuous vector-valued polynomials of degree  $p$  on a subdivision  $T_h$  of the domain into non-overlapping elements such that  $\Omega = \bigcup_{\kappa \in T_h} \kappa$ . Thus, the solution and test function space is defined by



$$\mathbf{V}_h^p = \left\{ \mathbf{v} \in L^2(\Omega) \mid \mathbf{v}|_\kappa \in P_p, \kappa \in T_h \right\},$$

133 where  $P_p$  is the space of polynomial functions of degree at most  $p$ . The discrete problem then takes  
 134 the following form: find  $\mathbf{q}_h \in \mathbf{V}_h^p$  such that

$$\begin{aligned} \sum_{\kappa \in T_h} \left\{ \int_{\kappa} \mathbf{v}_h^T \Gamma \frac{\partial \mathbf{q}_h}{\partial t} d\mathbf{x} - \int_{\kappa} \nabla \mathbf{v}_h^T \cdot \mathbf{F}(\mathbf{q}_h) d\mathbf{x} \right. \\ \left. + \int_{\partial\kappa \setminus \partial\Omega} \mathbf{v}_h^{+T} \mathbf{H}_i(\mathbf{q}_h^+, \mathbf{q}_h^-, \mathbf{n}) ds + \int_{\partial\kappa \cap \partial\Omega} \mathbf{v}_h^{+T} \mathbf{H}_b(\mathbf{q}_h^+, \mathbf{q}_h^b, \mathbf{n}) ds \right\} = 0 \end{aligned} \quad (11)$$

135 for all  $\mathbf{v}_h \in \mathbf{V}_h^p$ , where  $\mathbf{H}_i(\mathbf{q}_h^+, \mathbf{q}_h^-, \mathbf{n})$  and  $\mathbf{H}_b(\mathbf{q}_h^+, \mathbf{q}_h^b, \mathbf{n})$  are numerical flux functions defined on  
 136 interior and boundary faces, respectively.  $\mathbf{H}_i$  takes into account the possible discontinuities of  $\mathbf{q}_h$  at  
 137 element interfaces. On interior edges  $\partial\kappa \setminus \partial\Omega$ ,  $\mathbf{H}_i$  depends on the elements interior state  $\mathbf{q}_h^+$  and on the  
 138 neighbouring elements state  $\mathbf{q}_h^-$ . On boundary edges  $\partial\kappa \cap \partial\Omega$ ,  $\mathbf{H}_b$  depends on the interior state  $\mathbf{q}_h^+$  and  
 139 a consistent boundary state  $\mathbf{q}_h^b$ . We note that  $\mathbf{H}_b$  may be different from  $\mathbf{H}_i$ .

Given a set of basis functions  $\psi_j$ ,  $j = 1, \dots, N$ , of the discrete function space  $\mathbf{V}_h^p$  with  $N = \#\mathbf{V}_h^p$   
 we define the residual vector  $\mathbf{R} = \{(\mathcal{R}(\mathbf{q}_h), \psi_j)\}_{j=1, \dots, N}$  where

$$(\mathcal{R}(\mathbf{q}_h), \mathbf{v}_h) \equiv \int_{\kappa} \nabla \mathbf{v}_h^T \cdot \mathbf{F}(\mathbf{q}_h) d\mathbf{x} - \int_{\partial\kappa \setminus \partial\Omega} \mathbf{v}_h^{+T} \mathbf{H}_i(\mathbf{q}_h^+, \mathbf{q}_h^-, \mathbf{n}) ds - \int_{\partial\kappa \cap \partial\Omega} \mathbf{v}_h^{+T} \mathbf{H}_b(\mathbf{q}_h^+, \mathbf{q}_h^b, \mathbf{n}) ds,$$

140 for all  $\mathbf{v}_h \in \mathbf{V}_h^p$ . Then the spatial DG discretization of Eq. (11) results in the following global system  
 141 of equations:

$$\mathbf{M}_\Gamma \frac{d\mathbf{Q}}{dt} - \mathbf{R} = 0, \quad (12)$$

142 where  $\mathbf{Q}$  is the global vector of degrees of freedom (dof) with  $\mathbf{q}_h = \sum_{j=1, \dots, N} Q_j \psi_j$ .  $\mathbf{R}$  is the  
 143 residual vector as defined above and  $\mathbf{M}_\Gamma$  stands for the discretization of the first integral of Eq. (11).

Hence,  $\mathbf{M}_\Gamma$  is a block diagonal matrix where the block corresponding to one element couples all the dof of all variables within the element (the coupling among dof of different variables is due to the action of  $\Gamma$ ).

### 3.1. Boundary Conditions

When  $\partial\kappa$  belongs to  $\partial\Omega$  the boundary fluxes, denoted by  $\mathbf{H}_b(\mathbf{q}^+, \mathbf{q}^b, \mathbf{n})$ , are chosen to weakly prescribe the boundary conditions of the problem. Here,  $\mathbf{n}$  is the unit outward normal vector,  $\mathbf{q}^+$  is the interior state at the boundary and  $\mathbf{q}^b$  is computed according to the conditions that must be satisfied on the boundary.

At far-field,  $\mathbf{H}_b$  is the numerical flux function  $\mathbf{H}_i(\mathbf{q}^+, \mathbf{q}^b, \mathbf{n})$ , where  $\mathbf{q}^b$  is computed by imposing a set of simplified non-reflecting boundary conditions [6] to minimize spurious reflections. In particular at the inflow boundary the state  $\mathbf{q}^b$  has the same pressure as  $\mathbf{q}^+$ , whereas the velocity vector and the temperature is prescribed based on the freestream values. Conversely, at the outflow boundary, the state  $\mathbf{q}^b$  has the same temperature and velocity vector as  $\mathbf{q}^+$ , whereas the pressure is prescribed based on the freestream value. We remark that the simplified non-reflecting boundary conditions require a far-field boundary well far away from the aerodynamic surface in order to get efficient and accurate solutions.

At solid walls,  $\mathbf{H}_b$  is the inviscid flux function in the direction normal to the wall  $\mathbf{F}(\mathbf{q}^b) \cdot \mathbf{n}$ , where  $\mathbf{q}^b$  has the same pressure and temperature as  $\mathbf{q}^+$ , whereas the velocity vector  $\mathbf{v}^b = \mathbf{v}^+ - (\mathbf{v} \cdot \mathbf{n})^+ \mathbf{n}$  ensures that the normal velocity component is zero on the boundary,  $(\mathbf{v} \cdot \mathbf{n})^b = 0$ .

### 3.2. Flux difference splitting

The numerical flux  $\mathbf{H}_i(\mathbf{q}^+, \mathbf{q}^-, \mathbf{n})$  appearing in Eq. (11) is computed based on a preconditioning of the artificial dissipation term of the Roe's approximate Riemann solver [27]. In terms of primitive quantities  $\mathbf{q}$ , the value of  $\mathbf{H}_i$  at each face is given by

$$\mathbf{H}_i(\mathbf{q}^+, \mathbf{q}^-, \mathbf{n}) = \frac{1}{2} \left( \mathbf{F}(\mathbf{q}^+) \cdot \mathbf{n} + \mathbf{F}(\mathbf{q}^-) \cdot \mathbf{n} - \tilde{\mathbf{F}}_\Gamma(\mathbf{q}^+, \mathbf{q}^-, \mathbf{n}) \right), \quad (13)$$

166 where  $\tilde{\mathbf{F}}_\Gamma$  is given by

$$\tilde{\Gamma} |\tilde{\mathbf{A}}_\Gamma| \Delta \mathbf{q}. \quad (14)$$

167 Here,  $\Delta \mathbf{q} = \mathbf{q}^- - \mathbf{q}^+$  and the matrix  $|\tilde{\mathbf{A}}_\Gamma|$  is defined in terms of the preconditioned eigenvalues and  
168 eigenvectors by

$$|\tilde{\mathbf{A}}_\Gamma| = \tilde{\mathbf{T}}_\Gamma |\tilde{\Lambda}_\Gamma| \tilde{\mathbf{T}}_\Gamma^{-1}.$$

169 The symbol  $\tilde{\phantom{x}}$  denotes that the matrices are computed using the Roe-averaged variables [28] and  
170 the subscript  $\Gamma$  that the diagonal matrix of eigenvalues and the modal matrix are derived from the  
171 preconditioned system, where  $\tilde{\Lambda}_\Gamma$  is the diagonal matrix of the preconditioned eigenvalues, and  $\tilde{\mathbf{T}}_\Gamma$   
172 diagonalizes the matrix  $\Gamma^{-1}(\frac{\partial \mathbf{F}}{\partial \mathbf{q}} \cdot \mathbf{n})$ . We note, that for the non-preconditioned system, Eq.(13) reduces  
173 to the standard Roe's flux difference splitting.

#### 174 4. TIME DISCRETIZATION OF THE PRECONDITIONED EULER EQUATIONS

175 The semidiscrete system Eq.(12) is discretized in time based on an explicit multistage time-stepping  
176 method. In order to overcome the restrictive explicit CFL stability limit (the Courant number is  
177 approximately equal to  $1/(2p + 1)$  for linear stability of TVD Runge-Kutta schemes, where  $p$  is the  
178 polynomial degree of the spatial discretization), both the local time-stepping and the preconditioning  
179 techniques have been used to improve the convergence speed to steady state solutions.

180 The solution is advanced from time  $t$  to time  $t + \Delta t$  with an  $s$ -stage SSP Runge-Kutta scheme [29],  
 181 given by

$$\begin{aligned} \mathbf{Q}^0 &= \mathbf{Q}^t, \\ \mathbf{Q}^i &= \sum_{k=0}^{i-1} \alpha_{ik} \mathbf{Q}^k + \beta_{ik} \Delta t \mathbf{M}_\Gamma^{-1} \mathbf{R}(\mathbf{Q}^k) \quad i = 1, 2, \dots, s, \\ \mathbf{Q}^{t+\Delta t} &= \mathbf{Q}^s, \end{aligned} \quad (15)$$

182 where  $i$  is the stage counter for the  $s$ -stage scheme and  $\alpha_{ik}$  and  $\beta_{ik}$  are the multistage coefficients  
 183 for the  $i$ th stage.

184 The local time step  $\Delta t$  on each element  $\kappa$  is computed by considering the following relation:

$$\Delta t = \frac{\sigma}{2p+1} \cdot \frac{|\kappa|}{\Lambda_c^x + \Lambda_c^y}, \quad (16)$$

185 where the preconditioned convective spectral radii  $\Lambda_c^x$  and  $\Lambda_c^y$  are defined as

$$\begin{aligned} \Lambda_c^x &= (|\bar{u}'| + \bar{c}'_x) \Delta S^x, \\ \Lambda_c^y &= (|\bar{v}'| + \bar{c}'_y) \Delta S^y. \end{aligned} \quad (17)$$

186 The variables  $\Delta S^x$  and  $\Delta S^y$  represent the projections of the element  $\kappa$  onto the  $x$  and  $y$  axis,  
 187 respectively, whereas  $\bar{u}'$ ,  $\bar{c}'_x$  and  $\bar{v}'$ ,  $\bar{c}'_y$  are obtained applying Equations (6) along the  $x$  and  $y$  directions  
 188 and using the mean values of the flow quantities on each element  $\kappa$ . Finally,  $p$  is the polynomial degree  
 189 of the spatial discretization and  $\sigma$  is a factor introduced to take into account that SSP can be more  
 190 efficient than TVD Runge-Kutta schemes.

## 5. RESULTS

In this section, we present some numerical results demonstrating the performance of the proposed preconditioned DG discretization for inviscid very low Mach number flows. To this end, we consider an inviscid flow past a NACA0012 airfoil at zero angle of attack comparing the preconditioned DG discretizations with and without perturbed variables. DG solutions on a triangular O-type grid, for different very low Mach numbers and using linear ( $P_1$ ), quadratic ( $P_2$ ) and cubic ( $P_3$ ) elements are performed. Fig. 1 shows the computational grid. The grid is composed of 1792 elements, and the far-field boundary is located far away from the aerodynamic surface. All computations are performed in double precision, storing 16 significant digits.

The computational results are organized in two subsections, one focusing on the convergence characteristics of the preconditioned Euler equations and the other on the accuracy of the converged solutions.

The residual histories of pressure,  $p$ , temperature,  $T$ , horizontal,  $u$ , and vertical,  $v$ , velocity components versus iteration number are shown to represent the convergence characteristics.

The accuracy of the converged solutions is analyzed both qualitatively and quantitatively. First, the normalized pressure fields are presented for a qualitative comparison. Then, for the quantitative analysis, the scaling of computed pressure fluctuations as the Mach number reduces is compared with the  $M^2$  theoretical scaling.

## 5.1. Effect of the perturbed variables on convergence characteristics

The residuals are measured in terms of the absolute value of the ratio between the dependent variable changes and the local time step, both computed for each element  $\kappa$  using the mean values of the flow quantities. The residual of the generic dependent variable,  $q$ , was defined as:

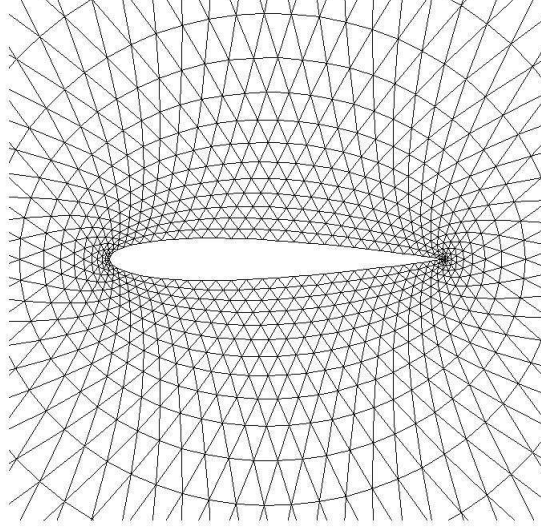


Figure 1: Computational Grid

$$Res(q) = \text{Max} \{ |\Delta(\bar{q})/\Delta t|_{\kappa}, \forall \kappa \in \Omega \} \quad \text{with } q = p, T, u, v. \quad (18)$$

213 The convergence histories of velocity are represented by the residuals of the horizontal velocity  
 214 component as similar histories are obtained for the vertical velocity component. Fig. 2 shows the  
 215 convergence characteristics of pressure (left column), temperature (middle column) and velocity (right  
 216 column) at  $M = 10^{-2}$ ,  $M = 10^{-4}$  and  $M = 10^{-6}$ , for linear ( $P_1$  top row), quadratic ( $P_2$  middle row)  
 217 and cubic ( $P_3$  bottom row) elements, without the perturbed variables. The residuals are normalized  
 218 with respect to the residual at the first time step. Overall, we see that, for a given polynomial degree, all  
 219 the convergence characteristics have the same convergence speed, which is independent of the Mach  
 220 number. Nevertheless, the efficiency of the preconditioned scheme reduces due to the CFL stability

221 condition.

222 Furthermore in Fig. 2 the influence of cancellation error on the residual decay can be clearly  
 223 seen. Examining the convergence histories of pressure, temperature, and velocity we can make two  
 224 observations. The first is that, for a given polynomial degree, the lower the Mach number, the smaller  
 225 the residual decay. The second is that, for a given Mach number, the higher the polynomial degree, the  
 226 smaller the reduction of the residual, even if this influence is less evident than the first.  
 227 However, both the influence of Mach number and polynomial degree on the decrease of the residual did  
 228 not allowed to obtain a solution at the lowest Mach number  $M = 10^{-6}$  using the highest polynomial  
 229 degree  $P_3$ .

230

231 Figure 3 shows the convergence characteristics with the perturbed variables. The residuals are  
 232 not normalized in order to highlight for the dependence of convergence characteristics on the  
 233 Mach number. We see that all the residuals decrease as the Mach number reduces. Specifically, the  
 234 convergence of pressure and temperature scale as  $O(M^3)$ , while the residual of velocity scales as  
 235  $O(M^2)$ . Then, as from Eq. (16) and Eq. (17) the order of magnitude of the local time stepping is  
 236  $O(M^{-1})$ , due to the order given in Eq. (7), the resulting orders of magnitude of the computed pressure,  
 237 temperature and velocity changes are  $O(M^2)$ ,  $O(M^2)$  and  $O(M)$ , respectively, in perfect agreement  
 238 with the theoretical behaviour.

239 Figure 4 shows the convergence characteristics with the perturbed variables, obtained scaling the  
 240 residuals of pressure, temperature and velocity as follows:

$$\begin{aligned}
Res(p) &= Max \left\{ \frac{|\Delta \bar{p} / \Delta t|_{\kappa}}{M^3}, \forall \kappa \in \Omega \right\}, \\
Res(T) &= Max \left\{ \frac{|\Delta \bar{T} / \Delta t|_{\kappa}}{M^3}, \forall \kappa \in \Omega \right\}, \\
Res(u) &= Max \left\{ \frac{|\Delta \bar{u} / \Delta t|_{\kappa}}{M^2}, \forall \kappa \in \Omega \right\}.
\end{aligned} \tag{19}$$

241 The plots show that the perturbed variables do not affect the convergence speed in comparison to  
 242 the non-perturbed solution, Fig. 2. We notice that the residual decay of pressure and velocity are now  
 243 independent of the Mach number.

244 Different is the case of the temperature. We see that even if we use the perturbed variables, the  
 245 residual of temperature reduces less as compared to the residual of pressure because they stagnate  
 246 at a level closer to the starting value. In particular, the decay of the temperature residual strongly  
 247 reduces when Mach number approaches zero. The reason of this behaviour can be found in the order  
 248 of magnitude of the convective fluxes as the Mach number approaches zero. Due to the orders of  
 249 magnitude of the non-dimensionalized quantities, Eq. (7), and considering that  $p' \sim O(M^2)$ , the  
 250 convective fluxes in the  $x$  and  $y$  direction Eq. (9) can be expressed as follows:

$$\mathbf{f}, \mathbf{g} \sim \begin{pmatrix} O(M) \\ O(M^2) \\ O(M^2) \\ O(M) + O(M^3) \end{pmatrix}.$$

251

252 We see that the range of the order of magnitude of the flux in the energy equation is wider than that  
 253 in the other equations. Thereby, the temperature suffers more from the cancellation problem than the  
 254 other variables [23].



255 The dependency of the residual reduction on the polynomial degree is the same previously observed  
256 without the perturbed variables.

257 Furthermore, we note that, using the perturbed variables, while the residual decay of pressure and  
258 velocity is sufficient enough to obtain accurate flow variable distributions, the lowest level of residual  
259 reduction of the temperature shows a strong effect of the cancellation error and this not always allowed  
260 to compute accurate temperature fields.

261 Finally, we observe that the explicit scheme results in an inefficient solution technique even  
262 using preconditioning. This is due to the restrictive limitations on the CFL number for higher order  
263 discretizations. A multigrid strategy might be implemented for the explicit time-stepping scheme in  
264 order to accelerate the convergence of the preconditioned Euler equations to the steady-state solution.

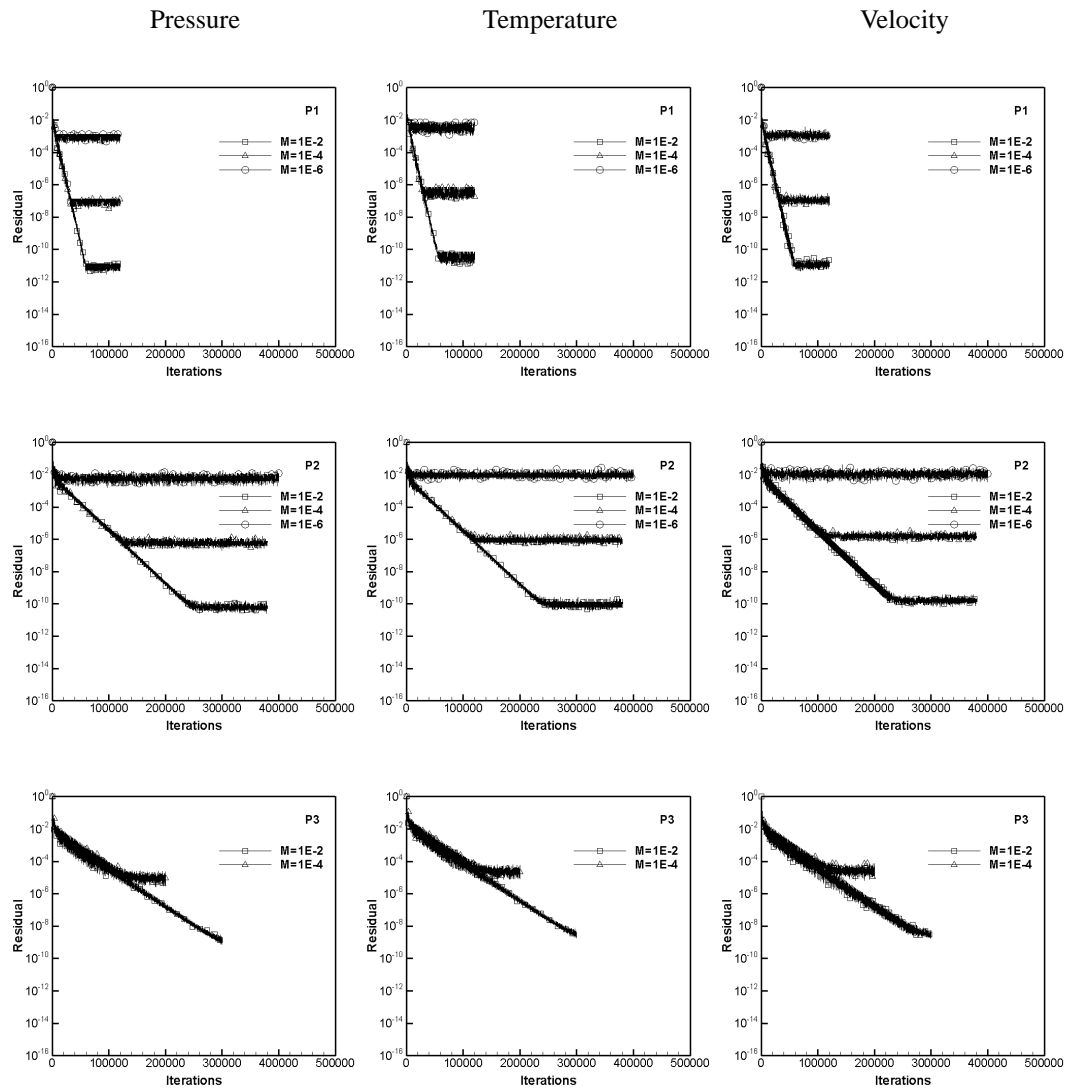


Figure 2: History of the nonlinear residuals vs. number of iteration steps for the pressure (left column), temperature (middle column) and velocity (right column), in normalized form without the perturbed variables at  $M = 10^{-2}$ ,  $M = 10^{-4}$  and  $M = 10^{-6}$ .  $P_1$  ( top row),  $P_2$  ( middle row) and  $P_3$  ( bottom row) elements.

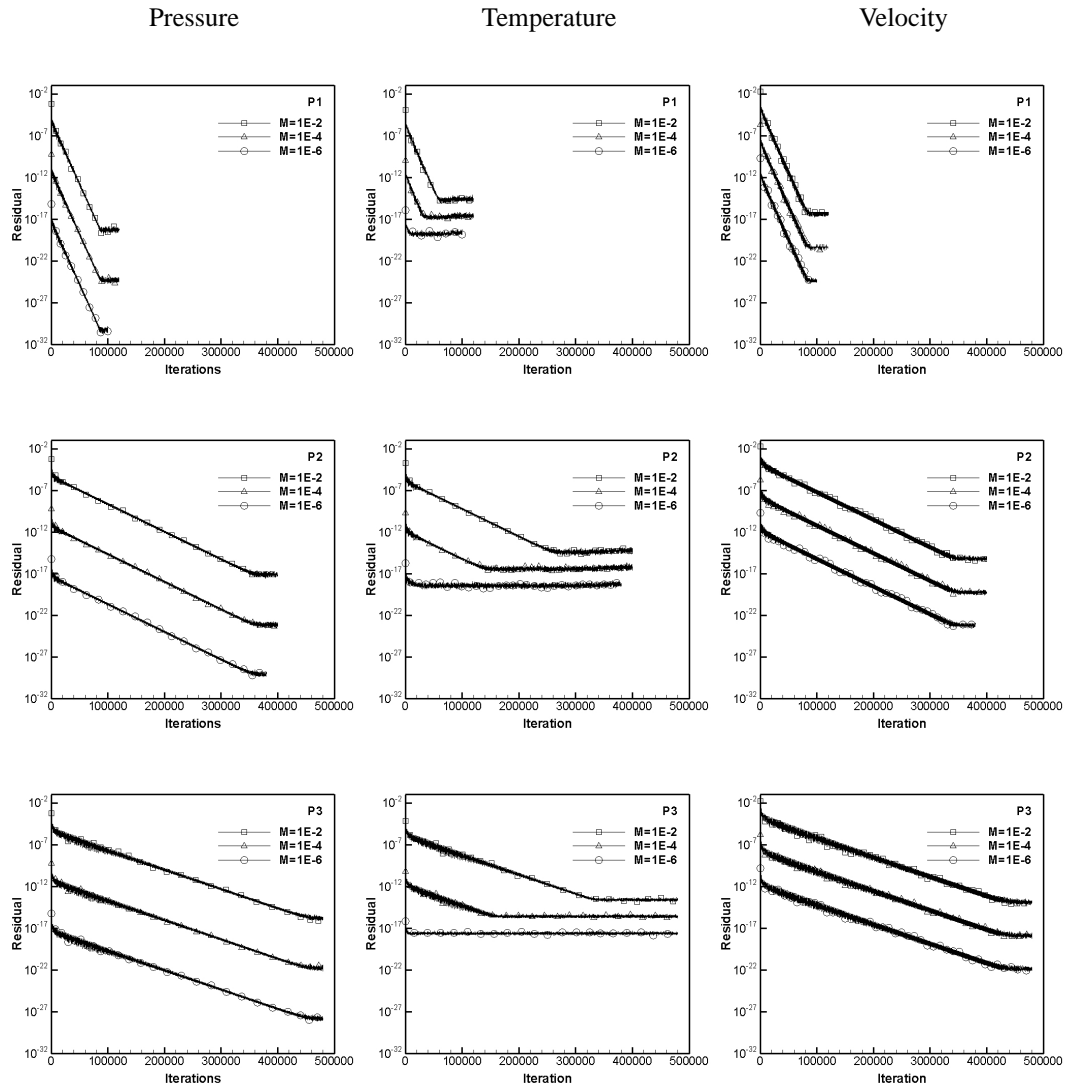


Figure 3: History of the nonlinear residuals vs. number of iteration steps for the pressure (left column), temperature (middle column) and velocity (right column), with the perturbed variables at  $M = 10^{-2}$ ,  $M = 10^{-4}$  and  $M = 10^{-6}$ .  $P_1$  (top row),  $P_2$  (middle row) and  $P_3$  (bottom row) elements.

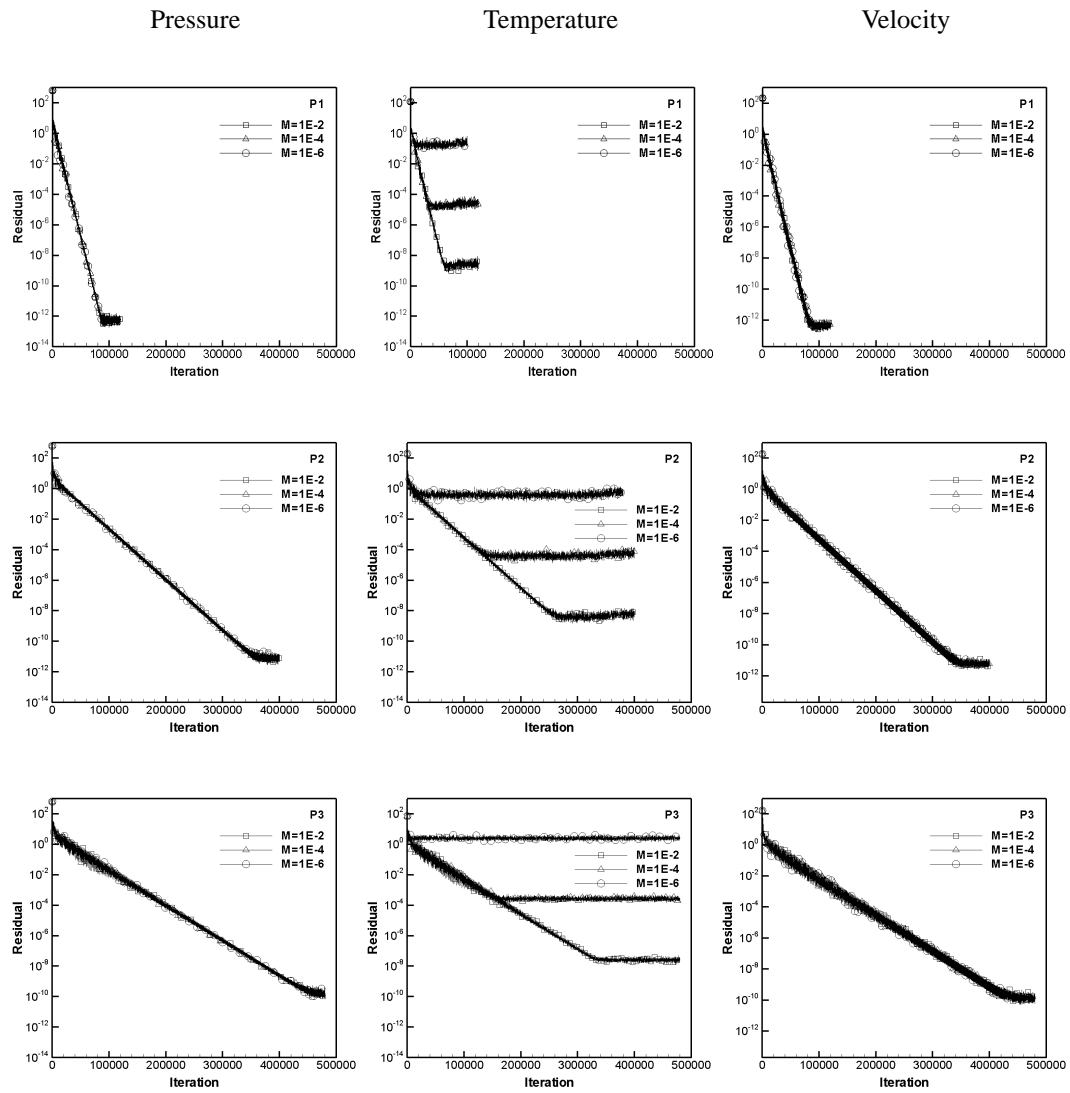


Figure 4: History of the nonlinear residuals vs. number of iteration steps for the pressure (left column), temperature (middle column) and velocity (right column), in scaled form with the perturbed variables at  $M = 10^{-2}$ ,  $M = 10^{-4}$  and  $M = 10^{-6}$ .  $P_1$  ( top row),  $P_2$  ( middle row) and  $P_3$  ( bottom row) elements.

265 5.2. *Effect of the perturbed variables on the solution accuracy*

266 5.2.1. *Normalized isolines* In the following we present the contour plots of the normalized pressure,  
 267  $p_{norm}$ , temperature,  $T_{norm}$ , and absolute value of velocity,  $|v|_{norm}$ . The normalized variable,  $q_{norm}$ ,  
 268 was defined as:

$$q_{norm} = (q - q_{min}) / (q_{max} - q_{min}),$$

269 where  $q = p, T, |v|$ . Figures 5 and 6 show the normalized contours of pressure (left column),  
 270 temperature (middle column) and velocity vector (right column) at  $M = 10^{-5}$ , using  $P_1$  (top row),  
 271  $P_2$  (middle row) and  $P_3$  (bottom row) elements, without and with the perturbed variables, respectively.  
 272 We see that on the basis of normalized pressure and absolute value of velocity isolines there is no  
 273 difference between the perturbed and the non-perturbed solutions, whereas isolines of temperature  
 274 begin to deteriorate using  $P_3$  elements and non-perturbated variables.

275 The solutions at  $M = 10^{-6}$ , see Figures 7 and 8, show more clearly how using the perturbed  
 276 variables improves the numerical accuracy in the low Mach number limit. Here, the  $P_1$  solutions  
 277 obtained using non-perturbated variables exhibit numerical oscillations, and the results worsen as the  
 278 polynomial degree increases. This is due to the higher number of computations performed when the  
 279 higher order approximations are used. In other words, the larger the number of computations with  
 280 rounding errors occurring at each computation, the worse the solution. Like for the  $P_3$  solution at  
 281  $M = 10^{-6}$ , it was not possible to obtain a converged solution for lower Mach numbers, regardless of  
 282 the polynomial degree. From these results we see that the perturbed variables are fundamental to obtain  
 283 convergence of continuity and momentum equations at very low Mach numbers, although the energy  
 284 equation still does not converge. In fact the perturbed formulation of the Euler equations allowed to  
 285 obtain accurate pressure and velocity isolines even for extremely low Mach number adiabatic flows,

286  $M = 10^{-15}$ , see Figure 9, independently of the polynomial degree of the numerical solution, thus  
 287 extending the DG scheme to the incompressible limit.

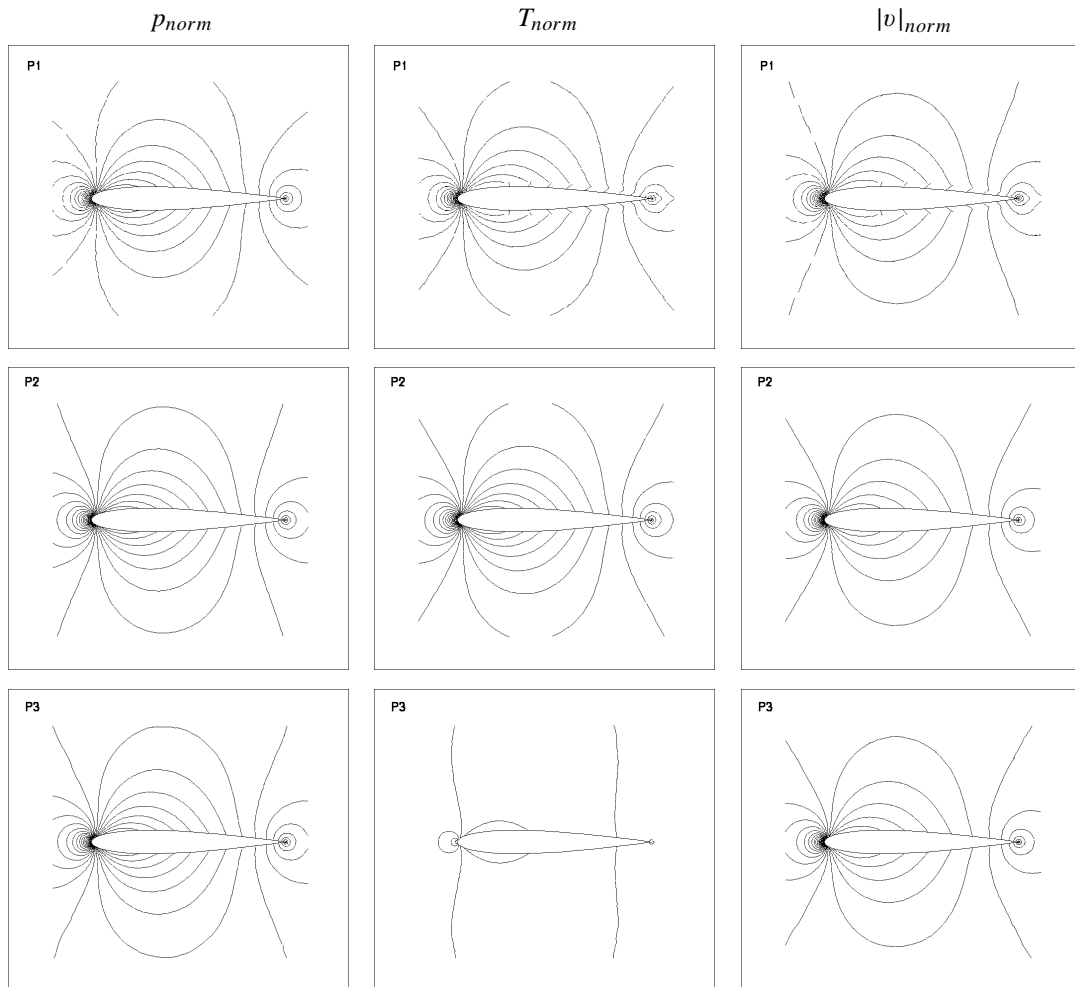


Figure 5: Non-perturbed method: test at  $M = 10^{-5}$ . Contours of normalized pressure (left column), temperature (middle column) and velocity (right column).  $P_1$  ( top row),  $P_2$  ( middle row) and  $P_3$  ( bottom row) elements.

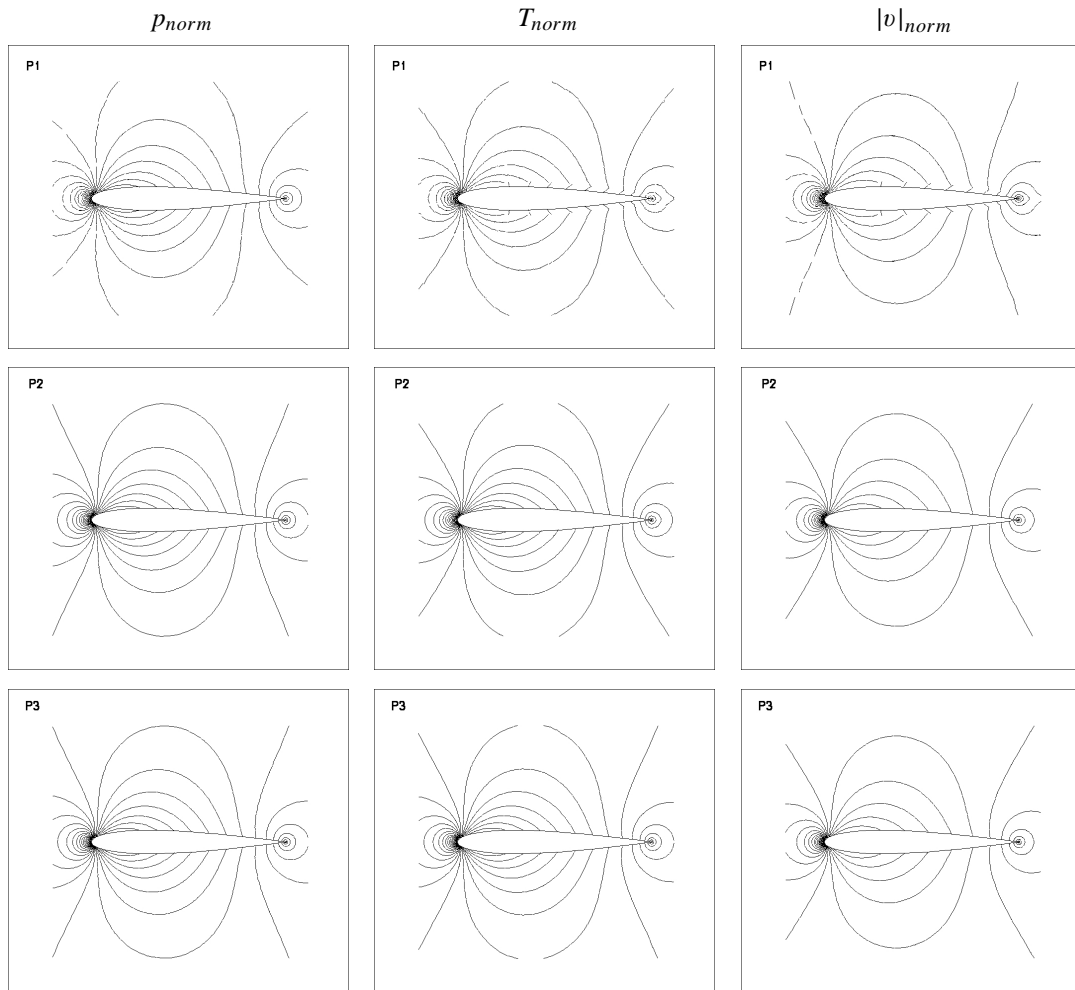


Figure 6: Perturbed method: test at  $M = 10^{-5}$ . Contours of normalized pressure (left column), temperature (middle column) and velocity (right column).  $P_1$  ( top row),  $P_2$  ( middle row) and  $P_3$  ( bottom row) elements.

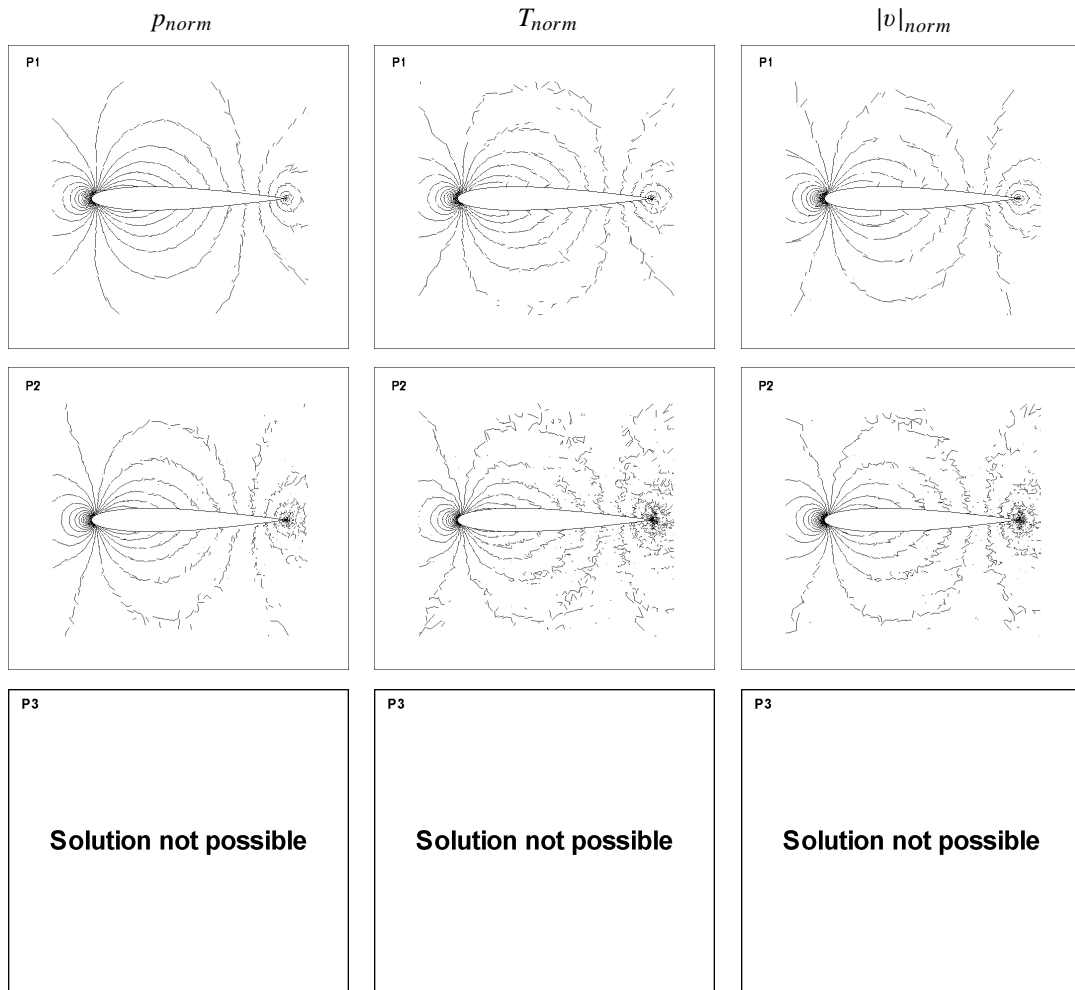


Figure 7: Non-perturbed method: test at  $M = 10^{-6}$ . Contours of normalized pressure (left column), temperature (middle column) and velocity (right column).  $P_1$  ( top row),  $P_2$  ( middle row) and  $P_3$  ( bottom row) elements.



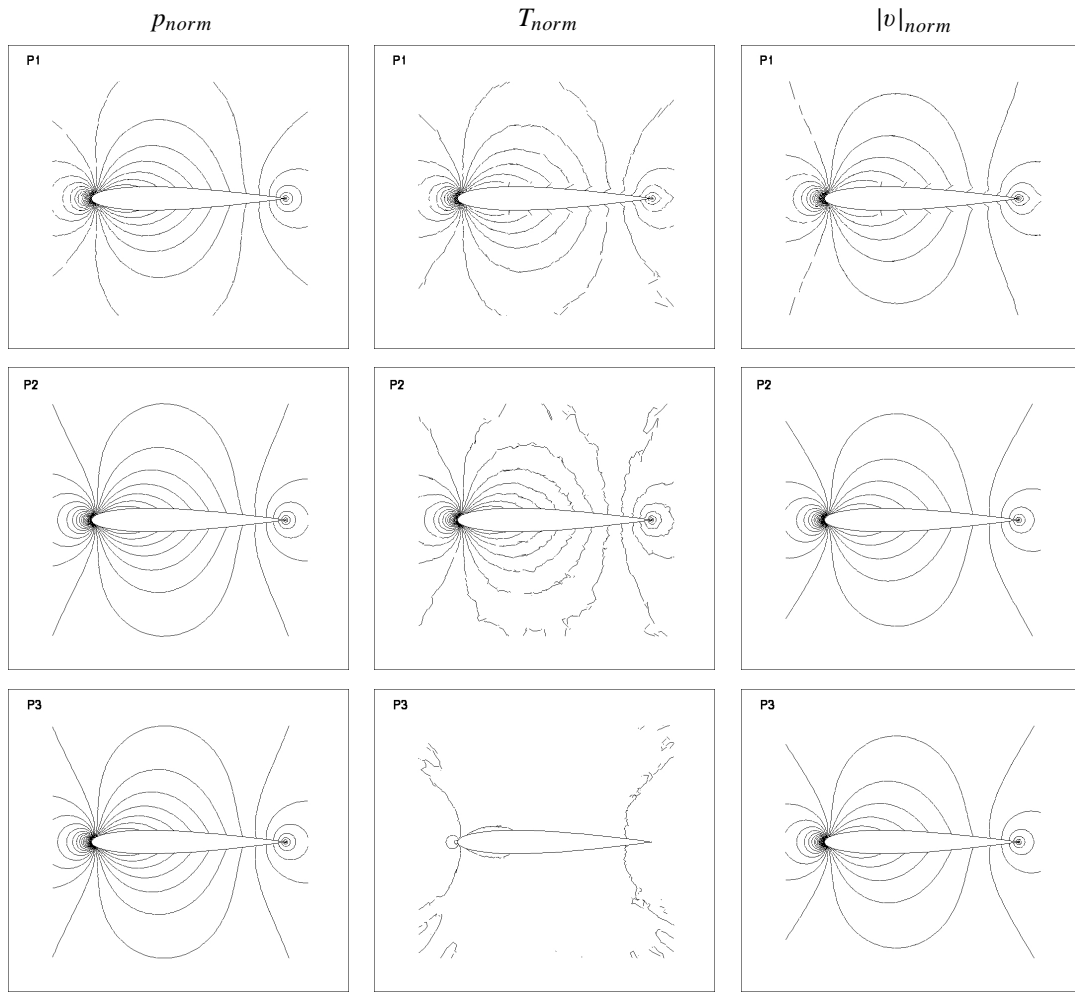


Figure 8: Perturbed method: test at  $M = 10^{-6}$ . Contours of normalized pressure (left column), temperature (middle column) and velocity (right column).  $P_1$  ( top row),  $P_2$  ( middle row) and  $P_3$  ( bottom row) elements.

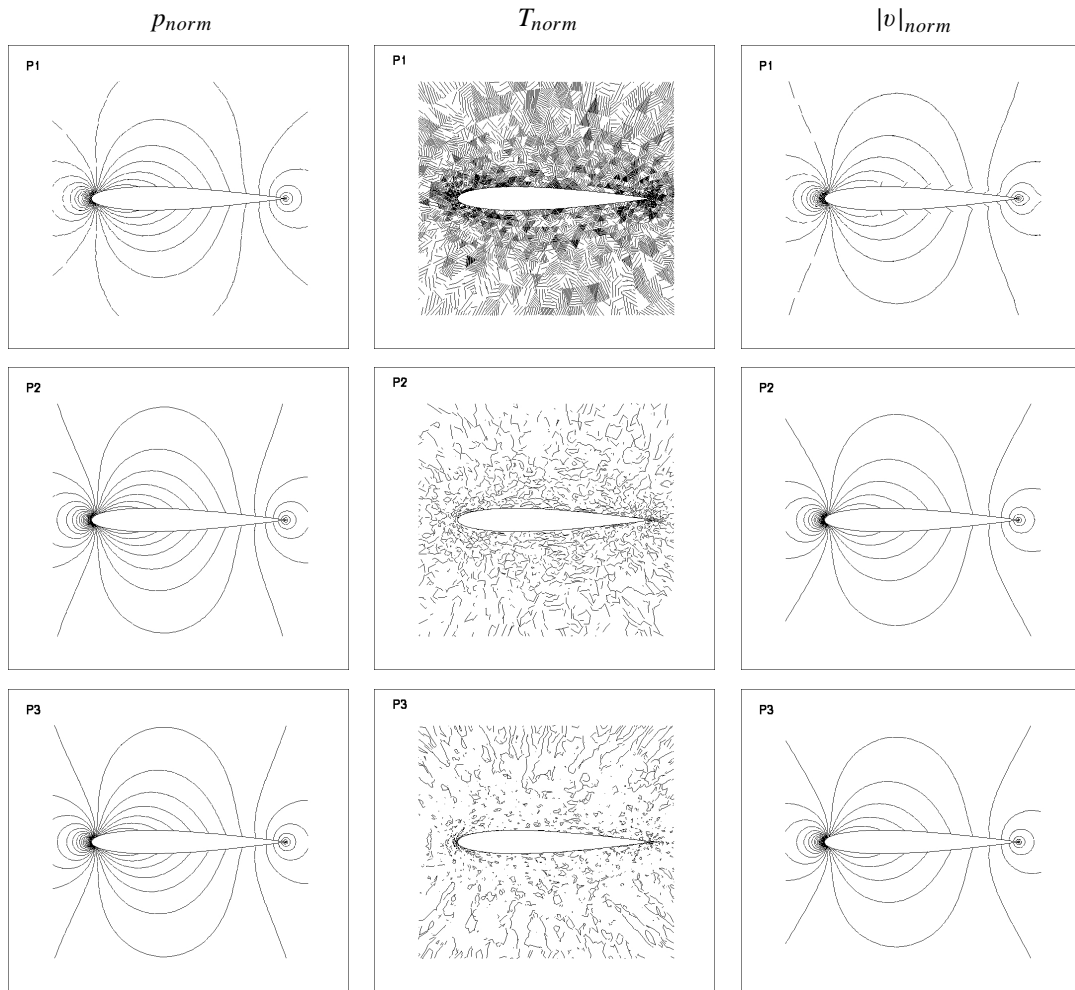


Figure 9: Perturbed method: test at  $M = 10^{-15}$ . Contours of normalized pressure (left column), temperature (middle column) and velocity (right column).  $P_1$  ( top row),  $P_2$  ( middle row) and  $P_3$  ( bottom row) elements.

288 5.2.2. *Pressure fluctuations* Fig. 10 shows the pressure fluctuations  $(p_{\max} - p_{\min})/p_{\max}$  versus the  
 289 Mach number at  $M = 10^{-2}$ ,  $M = 10^{-4}$ ,  $M = 10^{-6}$  and  $M = 10^{-15}$ , using  $P_1$ ,  $P_2$  and  $P_3$  elements,  
 290 with the perturbed variables. We see that the perturbed formulation of the Euler equations preserves

the accuracy of the solutions at extremely low Mach numbers. In perfect agreement with the theory,  
the pressure fluctuations scale exactly with the square of the Mach number down to  $M = 10^{-15}$ .

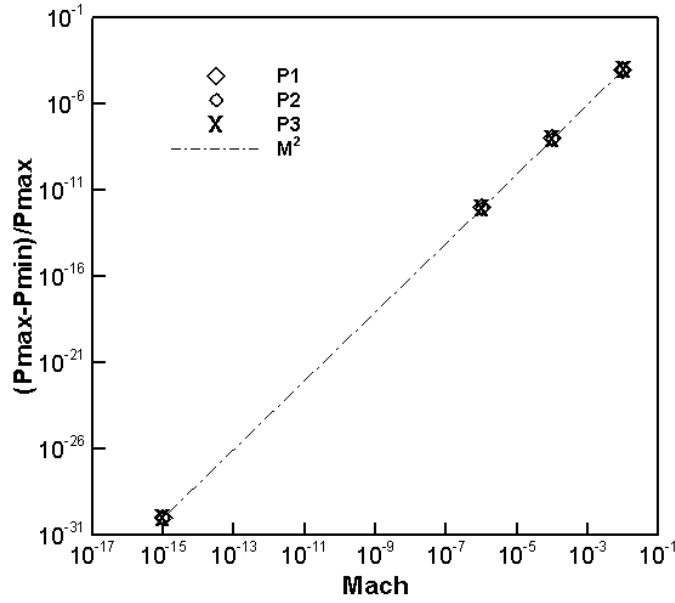


Figure 10: Pressure fluctuations vs. Mach number for  $P_1$ ,  $P_2$  and  $P_3$  elements using perturbed variables. Dashed and dotted line displays the theoretical behavior of  $M^2$ .

## 6. CONCLUSIONS

In this work we have presented the main features of a preconditioned DG discretization for inviscid very low Mach number computations. The method solves the compressible Euler equations written in terms of primitive variables and iterates to steady-state using an explicit scheme. The algorithm employs the perturbed formulation of the governing equations and the low Mach number preconditioning of both the time-derivative term of the governing equations and of the numerical flux function (full preconditioning

299 approach).

300 Numerical results have been presented solving the 2D compressible Euler equations at different  
301 very low Mach numbers using linear, quadratic and cubic elements, with and without the perturbed  
302 variables. The perturbed formulation allowed to investigate on the relationship between convergence  
303 characteristics and Mach number. For a given polynomial degree, the convergence characteristics of  
304 continuity, momentum and energy equations were found independent of the Mach number, showing  
305 that the scaling of the computed pressure, temperature and velocity changes as Mach number  
306 reduces are in agreement with the  $M^2$ ,  $M^2$  and  $M$  theoretical scaling, respectively. Furthermore,  
307 for a given Mach number, it was shown that the residual decays reduce when polynomial degree  
308 increases even using perturbed variables. In all cases the convergence speed was not affected by the  
309 perturbed variables. Some convergence problems were found for the energy equation at very low Mach  
310 numbers due to cancellation errors. Nevertheless, it has been shown that the perturbed formulation  
311 is mandatory to obtain accurate pressure and velocity distributions at low Mach numbers, especially  
312 when computations are performed using high order representations of the unknowns.

## 313 REFERENCES

- 314 1. H. Luo and J. Baum, R. Lohner. A Fast p-Multigrid Discontinuous Galerkin Method for Compressible Flows at All Speeds.  
315 44th AIAA Aerospace Sciences Meeting and Exhibit, Reno, 2006.
- 316 2. M. Feistauer, V. Kucera. On a robust discontinuous Galerkin technique for the solution of compressible flow. J. Comput.  
317 Physics, Vol 224, Issue 1, pp. 208-221, 2007.
- 318 3. G. Volpe. Performance of compressible flow codes at low mach numbers. AIAA Journal, 31:49–56, 1993.
- 319 4. E. Turkel, A. Fiterman, B. van Leer. Preconditioning and the limit of the compressible to the incompressible flow equations  
320 for finite difference schemes. In: Caughey DA, Hafez MM, editors. Frontiers of Computational Fluid Dynamics. Wiley,  
321 Chichester, 1994:215-234, 1994.
- 322 5. H. Guillard and C. Viozat. On the Behavior of Upwind Schemes in the Low Mach Number Limit. Computers & Fluids,  
323 Vol. 28, pp. 63-86, 1999.
- 324 6. Radespiel, R.; Turkel, E.; Kroll, N.:Assessment of Preconditioning Methods. DLR-FB 95–29 (1995).
- 325 7. P. Moinier, M.B. Giles. Compressible Navier-Stokes Equations for Low Mach Number Applications. ECCOMAS  
326 Computational Fluid Dynamics Conference 2001, pages 1-14, Swansea, Wales, UK, September 4-7, 2001.
- 327 8. B. Müller, Influence of Inlet and Outlet Boundary Conditions in Internal Flow Computations at Low Mach Numbers, in  
328 Desideri, J.-A., Hirsch,C., Le Tallec,P., Pandolfi,M., Periaux,J. (Eds.), "Computational Fluid Dynamics '96", Proc. 3rd  
329 ECCOMAS CFD Conference, Paris, 9-13 Sept. 1996, John Wiley, Chichester, 1996, pp. 637-643.
- 330 9. E. Turkel. Review of Preconditioning Methods for Fluid Dynamics. Applied Numerical Mathematics, Vol. 12, pp. 257-284,  
331 1993.
- 332 10. E. Turkel. Preconditioning Techniques in Computational Fluid Dynamics. Annu. Re. Fluid Mech., Vol. 31, pp. 385-416,  
333 1999.
- 334 11. D. Lee and B. Van Leer. Progress in Local Preconditioning of the Euler and Navier-Stokes Equations. AIAA Paper 93-3328,  
335 1993.
- 336 12. D. Lee. Local Preconditioning of the Euler Equations and Navier-Stokes Equations. PhD Thesis, University of Michigan,  
337 1996
- 338 13. J. Weiss and W. A. Smith. Preconditioning Applied to Variable and Constant Density Flows. AIAA Journal , Vol.33, pp.  
339 2050-2057, 1995.
- 340 14. Y. H. Choi and C. L. Merkle. The Application of Preconditioning in Viscous Flows. J. Comput. Physics, Vol. 105, pp.  
341 207-233, 1993.
- 342 15. A. Nigro, Discontinuous Galerkin methods for inviscid low Mach number flows. DLR-IB 124–2008/1.

- 343 16. F. Bassi, C. De Bartolo, R. Hartmann and A. Nigro. A discontinuous Galerkin method for inviscid low Mach number flows.  
344 J. Comput. Physics, submitted, 2008.
- 345 17. J. Sesterhenn, B. Muller and H. Thomann. On the Cancellation Problem in Calculating Compressible Low Mach Number  
346 Flow. J. Comput. Physics. Vol 151, pp. 597-615, 1999.
- 347 18. B. Muller and P. Jenny. Improving the Reliability of Low Mach Number Flow Computations. CFD Journal, 9(1):518-528,  
348 2001.
- 349 19. R. Klein. Semi-Implicit Extension of a Godunov-Type Scheme Based on low Mach Number Asymptotics I: One-  
350 Dimensional Flow J. Comput. Phys. 121:213-237, 1995.
- 351 20. H. Bijl, P. Wesseling. Unified formulation for compressible and incompressible flows by using multi-integrated moments  
352 II: multi-dimensional version for compressible and incompressible flows. J. Comput. Phys. 141: 153-173, 1998.
- 353 21. H. Guillard, A. Murrone. On the behaviour of upwind schemes in the low Mach number limit: II. Godunov type schemes.  
354 Computers and Fluids 33: 655-675, 2004.
- 355 22. Schneider Th., Botta N., Geratz K.-J., Klein R., Extension of Finite Volume Compressible Flow Solvers to Multi-  
356 Dimensional, Variable Density Zero Mach Number Flow, J. Comput. Phys., 155: 248-286, 1999.
- 357 23. S. H. Lee. Convergence characteristics of preconditioned Euler Equations. J. Comput. Physics, Vol. 208, pp. 266-288,  
358 2005.
- 359 24. G. Hauke and T. J. R. Hughes. A comparative study of different sets of variables for solving compressible and  
360 incompressible flows. Comput. Methods Appl. Mech. Eng., 153:1-44, 1998.
- 361 25. D. Vigneron, G. Deliége, J.A. Essers "Low Mach Number Local Preconditioning For Unsteady Viscous Finite Volumes  
362 Simulations on 3D Unstructured Grids", ECCOMAS Computational Fluid Dynamics Conference 2006, pages 1-14, TU  
363 Delft, Netherland, 2006.
- 364 26. E. Turkel., Preconditioned Methods for Solving Incompressible and Low Speed Compressible Equations. J. Comput.  
365 Physics, Vol. 72, pp. 277-298, 1987
- 366 27. P.L. Roe. Characteristic Based Schemes for the Euler Equations. Annual Review of Fluid Mechanics, Vol. 18, pp. 337-365,  
367 1986.
- 368 28. P.L. Roe. Approximate Riemann Solvers, Parameter Vectors, and Difference Schemes. J. Comput. Physics., Vol 43, pp.  
369 357-352, 1981.
- 370 29. R. J. Spiteri and S.J. Ruuth. A new Class of Optimal High-Order Strong-Stability-Preserving Time Discretization  
371 Methods, Technical Report CS-2001-01, Acadia University, Wolfville, Nova Scotia, Canada, 2001.